

LIFT AND DRAG COEFFICIENTS FOR DIFFERENT MAGNUS ROTOR TYPES

KOEFICIENTI VZGONA IN UPORA ZA RAZLIČNE KONFIGURACIJE MAGNUSOVEGA ROTORJA

Marko Pezdevšek³¹

Keywords: Magnus effect, lift coefficient, drag coefficient, Ansys CFX, endplates, aspect ratio

Abstract

In this paper, the results of numerical simulations for various Magnus rotor configurations are presented. For each configuration, a blocked structured mesh was designed in ICEM CFD. Numerical simulations were conducted using Ansys CFX. The influence of the aspect ratio on the lift and drag coefficients depending on the speed ratio was investigated, as was the influence of endplates on a Magnus rotor. From the obtained results, it was concluded that adding endplates to a Magnus rotor increases the lift and drag coefficients.

Povzetek

V prispevku so predstavljeni rezultati numeričnih simulacij različnih konfiguracij Magnusovega rotorja. Za vsako konfiguracijo smo s programom ICEM CFD izdelali blokovne strukturirane numerične mreže. Numerične simulacije so bile izvedene s programskim paketom Ansys CFX. Preučili smo vliv geometrijskega razmerja Magnusovega rotorja na potek koeficienta vzgona in upora v odvisnosti od hitrostnega razmerja. V nadaljevanju smo še preučili vpliv končnih plošč. Iz rezultatov simulacij je razvidno, da uporaba končnih plošč povečuje koeficient vzgona in koeficient upora.

³¹ Corresponding author: Marko Pezdevšek, University of Maribor, Faculty of Energy Technology, Hočevarjev trg 1, 8270 Krško, E-mail address: marko.pezdevsek@um.si

1 INTRODUCTION

The Magnus effect was named after Heinrich Magnus, a German physicist who described the effect in 1852 in his research in the deflection of projectiles from firearms. The Magnus effect is present with a rotating object moving through a fluid. A rotating object (in our case a cylinder) experiences a deflection that can be explained by the difference in pressure of the fluid on opposite sides of the spinning object. The direction in which the deflection happens is related to the direction (clockwise or counterclockwise) of rotation. The forces that act on a rotating cylinder are seen in Figure 1; the lift force is defined as a force that is perpendicular to the free stream velocity while the drag force is parallel to the free stream velocity.

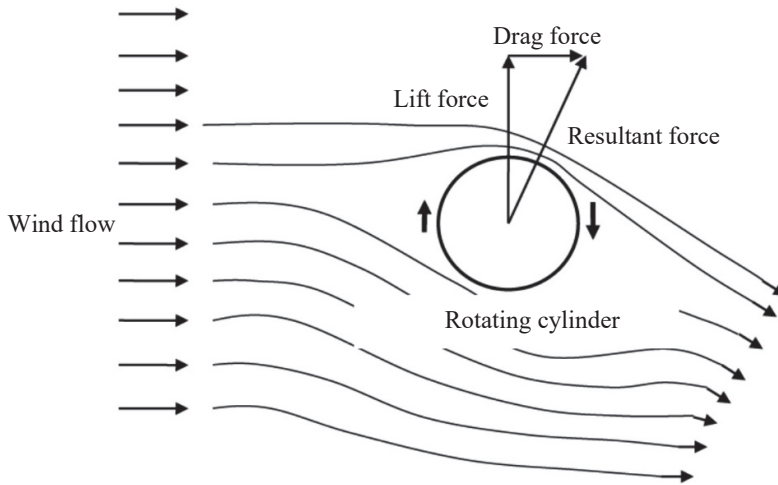


Figure 1: Forces acting on a rotating cylinder

The German engineer Anton Flettner was the first to build a ship that attempted to use the Magnus effect for propulsion. In 1924, he constructed the ship named "Backau", which had two large cylinders each 15 m in height and 3 m in diameter driven by a 37 kW motor. The ship would later be renamed "Baden Baden" and was used to cross the Atlantic Ocean, [1].

In recent years, research in Magnus rotors has increased, and several authors have covered this topic. Mandar Gadkari, [2], researched the Magnus effect using 2D numerical simulations. Niel Lopez, [3], conducted numerical simulations for different Magnus rotor types; at different aspect ratios, he investigated the effect that spirals, bumps and humps have on the lift and drag coefficient. Seyed Ali Kazemi, [4], used an airfoil geometry with rotating walls instead of the conventional cylinder shape; he conducted numerical simulations at various speed ratios and several angles of attack.

2 GEOMETRY, MESH, AND BOUNDARY CONDITIONS

2.1 Geometry

The aspect ratio (AR) is defined as the ratio between the height and diameter of a cylinder. Cylinders with aspect ratios of 2, 3, and 4 were modelled. Our goal was to investigate the dependency between AR and lift-drag coefficients. In the example in which we have AR=3, endplates were added to the cylinder. The diameter of the endplates was 2D. The size of the computational domain remained constant for all cases and was 1 m before, 2 m after, 1 m above and below the cylinder. The computational domain is shown in Figure 2.

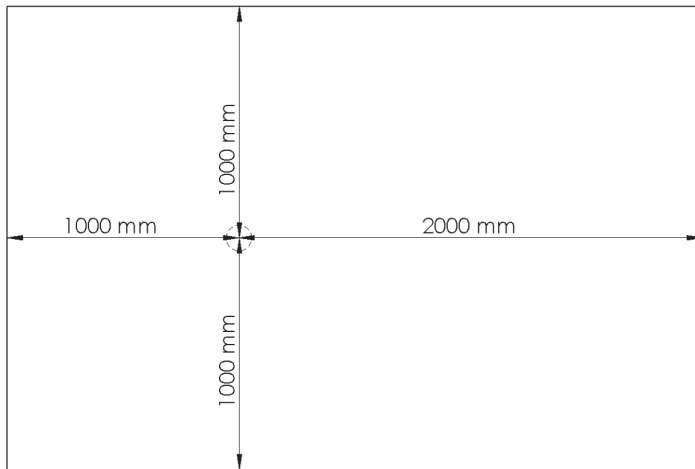


Figure 2: Computational domain

2.2 Mesh

For all the above-mentioned examples, a blocked structured mesh was created in ICEM CFD. The final mesh consisted of approximately 6 million elements. Figure 3 shows the mesh for AR=3; below the same figure, a section of the mesh is enlarged so we can better see the mesh distribution and size in the area near the cylinder walls.

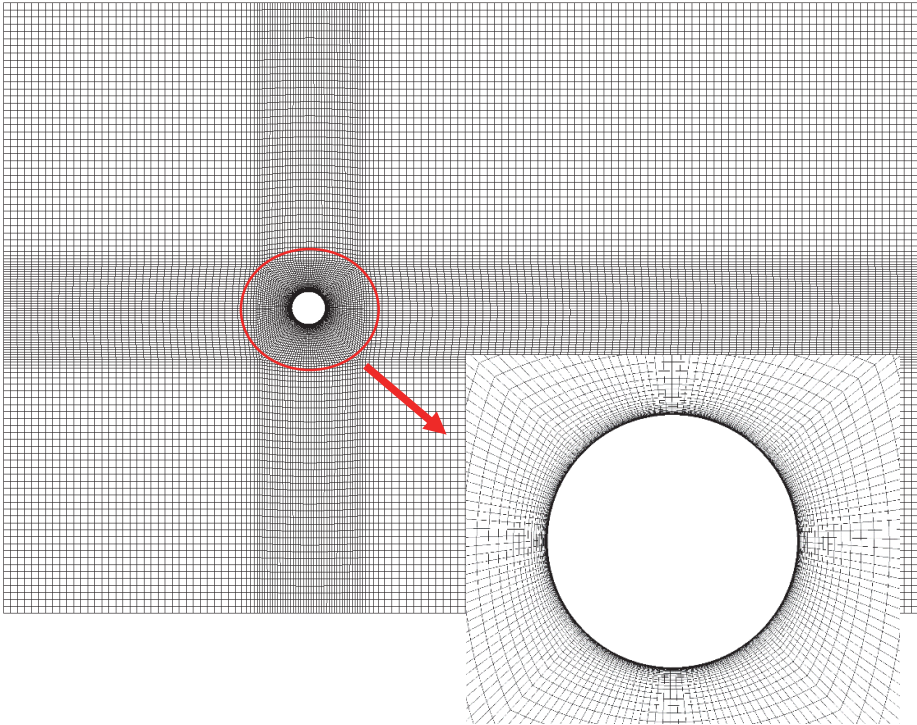


Figure 3: Blocked structured mesh with the magnified section at the bottom

The dimensionless value $y^+=1$ was taken into account during the mesh design phase. The element size near the cylinder wall was adjusted accordingly. An O-grid was incorporated into the basic design of the mesh; the expansion ratio perpendicular to the wall surface was set to 1.15. The height of the cylinder was described with 120 elements. The cylinder surface was described with 33,150 elements. Simulations have shown that the maximum y^+ is less than 4, which can be seen in Figure 4.

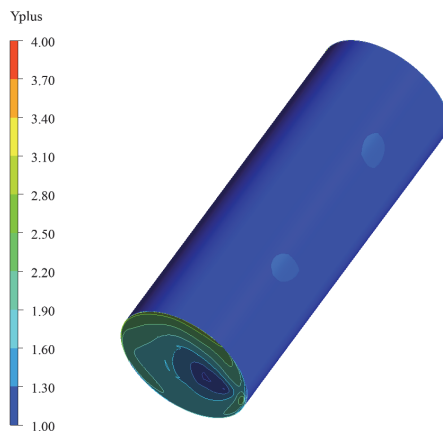


Figure 4: y^+ values

2.3 Boundary conditions

The following boundary conditions were applied. The left surface was defined as an inlet where an inlet velocity of 10 m/s was defined. The right surface was defined as an opening where the average static pressure 0 Pa was applied. The top and bottom walls were defined as stationary no-slip walls. The cylinder walls were defined as a rotating no-slip wall where an appropriate angular velocity was defined. All the above-mentioned boundary conditions can be seen in Figure 5.

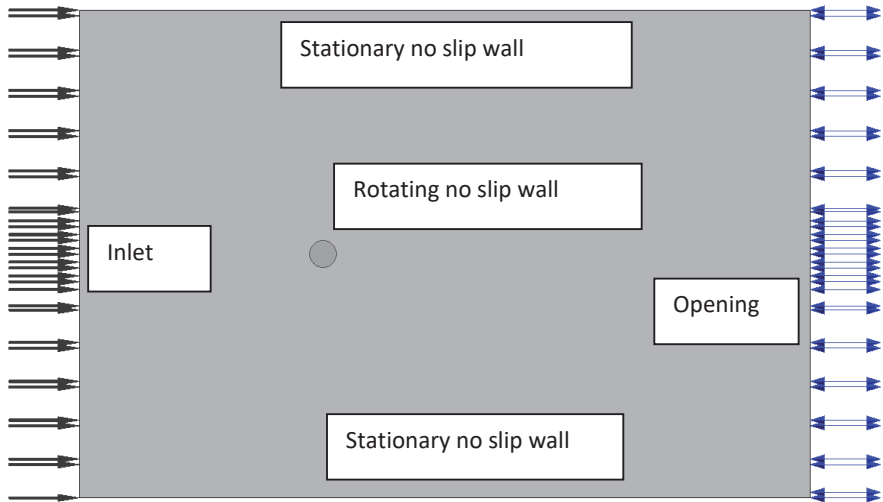


Figure 5: Applied boundary conditions

In Ansys CFX 17.1, we conducted steady-state simulations for speed ratios between 1 and 5 with a 0.5 step. The average RMS residuals were set at 10^{-5} . The SST turbulence model was used.

3 EXPERIMENT

The experimental measurements were completed in the wind tunnel of the Faculty of Energy Technology of the University of Maribor. The wind tunnel has a measuring cross-section of 2×2 m at which wind speeds of 25 m/s can be achieved. The general shape of the wind tunnel is a closed-loop design; at the bottom of the loop, there is a fan, while at the top of the loop there is the measuring section. The frame on which the whole structure (rotating cylinder, motors) is mounted to is bolted directly to the bottom surface of the wind tunnel. The horizontal axle is mounted with two bearings to the frame. The vertical shaft is powered by an electric motor, which is at the bottom of the shaft and is mounted in two places, which are seen in Figure 6. The cylinder is mounted to the vertical shaft. The experiment was conducted at a constant wind speed of 10 m/s. We changed the rpm of a cylinder with an AR=3 from 1000 rpm to 8000 rpm. The force was measured with an HBM U9C force gauge which was positioned perpendicular to the airflow. The position of the drive motor and force gauge can be seen in Figure 6.

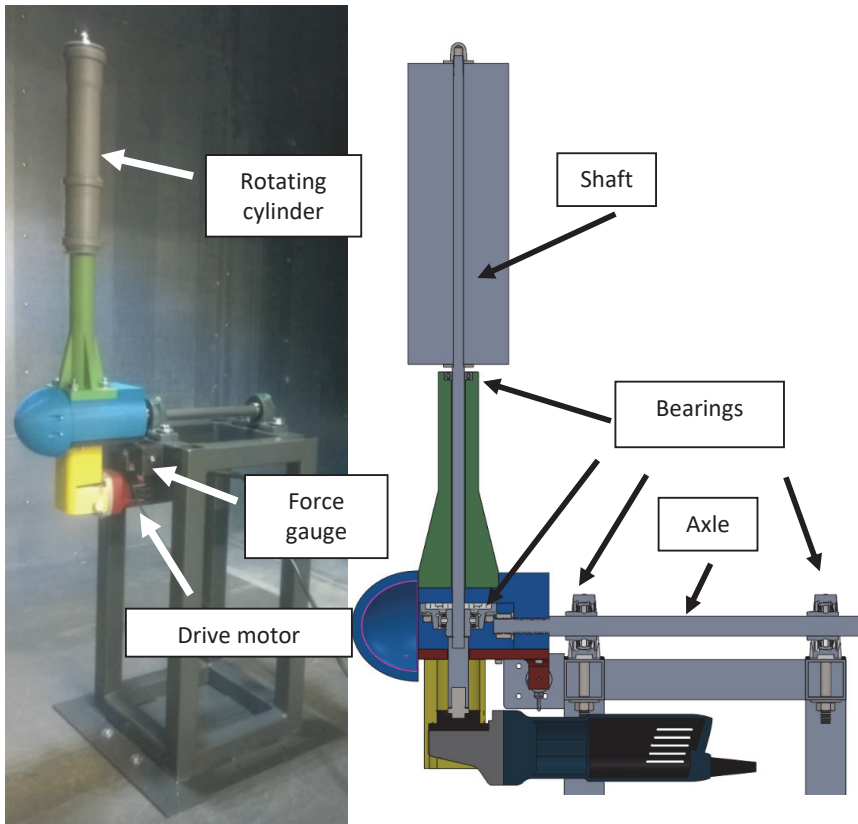


Figure 6: Position of components for the experiment

4 RESULTS

The lift coefficient is defined with the following equation:

$$C_l = \frac{F_l}{0.5 \rho A v_\infty^2} \quad (4.1)$$

Where:

- F_l – lift force [N],
- ρ – density [kg/m³],
- A – area of the cylinder field [m²],
- v_∞ – free stream velocity [m/s].

The drag coefficient is defined with the following equation:

$$C_d = \frac{F_d}{0.5 \rho A v_\infty^2} \quad (4.2)$$

Where:

- F_d – Drag force [N].

The aspect ratio is defined as the ratio between height and diameter of a cylinder.

$$AR = \frac{h}{2R} \quad (4.3)$$

Where:

h – cylinder height [m],

R – cylinder radius [m].

The area of the cylinder field is defined as the height multiplied with the diameter:

$$A = h2R \quad (4.4)$$

The speed ratio is defined as the ratio between the circumferential velocity and absolute velocity:

$$\lambda_2 = \frac{\Omega R}{v_\infty} \quad (4.4)$$

Where:

Ω – angular velocity [rad/s].

Figure 7 shows the lift coefficient as a function of the speed ratio. The figure contains experimental results and the results of CFD simulations at AR=3. At $\lambda_2 < 2$, we can see that the CFD results generally show good agreement with experimental data. The results deviate the most at $\lambda_2 = 2$, where the lift coefficient in the case of CFD simulations is still increasing, while the experimental data show that the maximum is already reached. At $\lambda_2 > 2$, the CFD results show good agreement with experimental data.

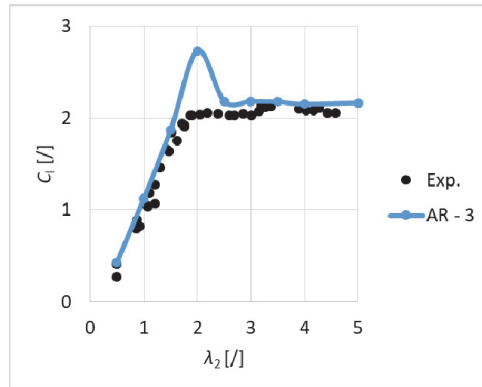


Figure 7: Lift coefficient as a function of the speed ratio

Figure 8 shows the lift coefficient (left) and the drag coefficient (right) as a function of the speed ratio. The figure contains the results of CFD simulation data at AR=2, 3, and 4. From Figure 8, we can conclude that the lift and drag coefficient increases with higher aspect ratios. At speed ratios higher than 3, we can observe that the lift coefficient remains constant, similarly as can be seen with the drag coefficient.

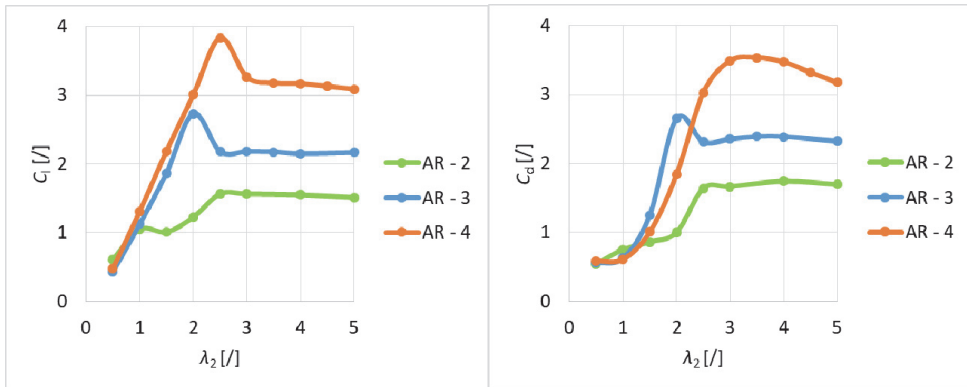


Figure 8: Lift coefficient (left) and drag coefficient (right) as a function of speed ratio for different aspect ratios

Figure 9 shows the lift coefficient (left) and the drag coefficient (right) as a function of the speed ratio. The figure shows the results of CFD simulations at AR=3, for the example with and without endplates. From the figure, we can see that with the use of endplates the lift and drag coefficient increases significantly. The maximum lift coefficient for the example without endplates is 2.8 at $\lambda_2=2$; with endplates, the coefficient rises to approximately 8 at $\lambda_2=4$. We can see a similar pattern with the drag coefficient which has a maximum value of 2.8 at $\lambda_2=2$ for the example without endplates. With the inclusion of endplates the maximum value rises to 9 at $\lambda_2=5$.

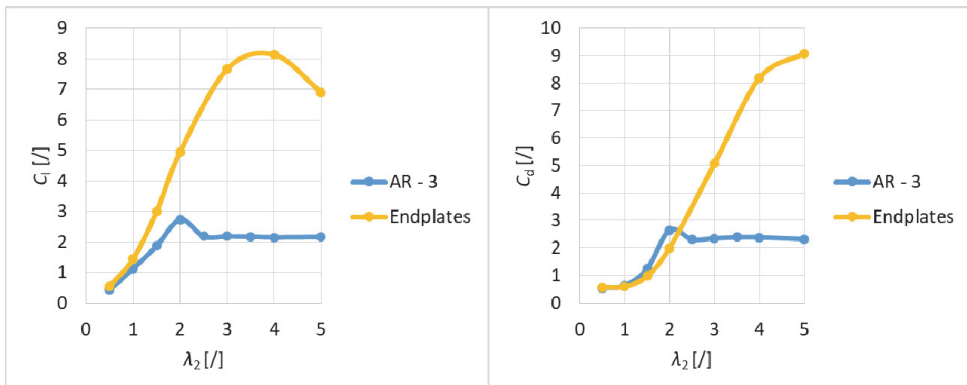


Figure 9: Lift coefficient (left) and drag coefficient (right) as a function of speed ratio for example with endplates (blue) and without endplates (yellow)

5 CONCLUSION

Several numerical simulations were performed for different Magnus rotor configurations. For each configuration, a blocked structured mesh in ICEM CFD was created. The simulations were conducted in Ansys CFX. We compared the results of CFD simulations for AR=3 to experimental data. At $\lambda_2 < 2$ and $\lambda_2 > 2$, the CFD results show good agreement with experimental data. At $\lambda_2 = 2$, the results deviate the most; in the case of CFD simulations, the lift coefficient is still increasing,

while the experimental data show that the maximum is reached. We compared the lift and drag coefficient depending on the speed ratio for different aspect ratios. The results show that with increasing the aspect ratio, the lift and drag coefficients increase. For a cylinder with $AR=3$, we compared CFD results for an example with and without endplates. The results show that the lift and drag coefficients increase significantly with the inclusion of endplates. In future work, we hope to include more experimental data and different cylinder designs.

6 REFERENCES

- [1] **J. Seifert:** A review of the Magnus effect in aeronautics, *Progress in Aerospace Sciences*, 55: 17-45, 2012
- [2] **M. Gadkari, V. Deshpande, S. Mahulkar, V. Khushalani, S. Pardhi, A.P. Kedar:** To study Magnus effect on Flettner rotor, *International research journal of engineering and technology*, Volume 4, Issue 2, 2017
- [3] **N. Lopez, B. Mara, B. Mercado, L. Mercado, M. Pascual, M.A. Promentila:** Design of modified Magnus wind rotor using computational fluid dynamics simulation and multi-response optimization, *Journal of renewable and sustainable energy* 7, 2015
- [4] **S.A. Kazemi, M.N. Ahmadabadi, A. Sedaghat, M. Saghafian:** Aerodynamic performance of a circulating airfoil section for Magnus systems via numerical simulation and flow visualization, *Energy*, 104, 2016

Nomenclature

(Symbols)	(Symbol meaning)
C_l	lift coefficient
F_l	lift force
ρ	density
A	area of the cylinder field
v_∞	free stream velocity
C_d	drag coefficient
F_d	drag force
AR	aspect ratio
h	cylinder height
R	cylinder radius
Ω	angular velocity
λ_2	speed ratio